# ARTICLES

## Chain Length Effects on Frictional Behavior of Confined Ultrathin Films of Linear Alkanes under Shear

**Asako Koike* and Makoto Yoneya**

*Hitachi Research Laboratory, Hitachi, Ltd. 7-1-1 Omika, Hitachi, Ibaraki 319-1292, Japan*

*Received: February 11, 1997; In Final Form: February 18, 1998*

Molecular dynamics simulations have been performed to study the effect of molecular chain length on frictional behavior of confined thin liquid films under shear. One of the walls confining the films, composed of linear alkanes (chain length 6−80), was moved at a constant velocity for two different pressures. The results indicate that there are distinct differences in frictional behavior under fast sliding velocity between low and high pressures. Under high pressure, interfacial slip appears between the moving wall, base, and the film, and shear stress doe not depend on the chain length. On the other hand, for low pressure, interlayer slips within the film appear in longer chains and shear stress depends on the chain length. In the interfacial and interlayer slip regions, more heat generated by friction is observed. Also, the interfacial shear stress is caused by the slider, interlayer shear stress is caused by interwined and locked layers, and both these stresses have maximum values. When the maximum interfacial shear stress is larger than the maximum interlayer shear stress, interlayer slips occur and in the reverse, interfacial slip occurs. When both maximum shear stresses are larger than the required shear stress for the film to have a uniform shear rate, there is no slip.

### I. Introduction

Investigations of tribological properties of organic thin films are important, because the films are widely used as lubricants to protect surfaces against damage by shearing friction. The introduction of sophisticated equipment such as the SFA (surface force apparatus)[1,2] and FFM (frictional force microscope)[3,4] has allowed tribological molecular behavior at the atomic scale to be studied, thus providing new insights into fundamental tribological behavior of organic thin films.[1−4] Measurements have shown when the distance between two surfaces is >50 nm, the confined liquid film follows Reynold's theory of lubrication.[5] Further, at >5 nm (∼10 molecular diameters of an *n*-alkane), the confined liquid film retains its bulk Newtonian behavior.[6−8] However, at <5 nm, the liquid has characteristic behavior not following any conventional law such as Newton's law of viscosity.[7,8] At low shear rate, the liquid film confined within a distance of several molecular diameters shows stick−slip motion. In the stick condition, the liquid film is expected to be frozen solidlike, and in the slip condition the film is expected to be a melt due to the shear stress.[7,8] This behavior depends on molecular structure, such as whether films are branched or linear molecules, and on sliding velocities. When the sliding velocities are higher than a critical velocity, the stick−slip motion vanishes. Further, it is known that the effective viscosities of the confined liquid film are several orders of magnitude larger than those of bulk and that they decrease with increasing shear rate according to a power law scaling.[9]

Computer simulations also have been used to investigate tribological behavior of thin films.[10−25] In shear simulations of the bead−spring liquid model confined between two solid walls, crystalline or glassy order was induced with wall separation of a few molecular diameters, which was interpreted as causing the stick condition. Power law scaling for viscosity and shear rate has also been examined.[15−17] The viscosity of a confined thin liquid film composed of Lennard−Jones (L−J) particles was observed to differ depending on the distance from the walls[11] and it increased largely with ordering of discrete layers.[19,20] It was also found that the slip occurred between layers within the film, if the film−wall interactions were strong.[21,22] However, an increase of viscosity was not observed for butane or longer main-chain molecules than butane.[23] For molecular structure, (e.g., branched and linear alkanes), though no difference in solvation force was observed,[24] a difference in shear stress was seen when the wall−liquid film interactions were strong.[25]

In summary, we can say the characteristic molecular behavior for a confined liquid film of several molecular diameters (e.g., stick−slip motion) and effects of molecular structure (e.g., branched and linear alkanes) at the low shear rate are beginning to be understood by experimental and computational approaches. At a sufficiently low shear rate and for a thick film, the confined molecules are well known to behave like a Newtonian liquid. On the other hand, in the thin films <5 nm (10 molecular diameters) and thicker than 2.5 nm (several molecular diameters), the molecules do not behave like a Newtonian liquid under high shear rate, although they do behave like a Newtonian liquid under low shear rate without stick−slip motions. Unfortunately the molecular behaviors under these conditions are not well understood.[26] In the present study, we have carried out simulations of thin confined liquid films thinner than 5 nm and thicker than 2.5 nm under shear. The simulations assumed two solid walls and were carried out for two values of pressure.

S1089-5647(97)00529-4 CCC: $15.00 
Published on Web 04/22/1998

**TABLE 1: Potential Function Parameters of Hydrocarbon Atoms**

| parameter | value | parameter | value |
|---|---|---|---|
| $k_b$ | 135.1 (MJ/mol/nm$^2$) | $b_0$ | 0.153 (nm) |
| $k_\theta$ | 460 (kJ/mol/rad$^2$) | $\theta_0$ | 1.936 (rad) |
| $C_0$ | 9.2789 (kJ/mol) | $C_1$ | 12.1557 (kJ/mol) |
| $C_2$ | −13.1201 (kJ/mol) | $C_3$ | −3.0597 (kJ/mol) |
| $C_4$ | 26.2403 (kJ/mol) | $C_5$ | −31.4950 (kJ/mol) |
| $\epsilon/k$ ($CH_3$) | 70.4 (K) | $\epsilon/k$ ($CH_2$) | 90.7 (K) |
| $\sigma$ ($CH_3$) | 0.3965 (nm) | $\sigma$ ($CH_2$) | 0.3786 (nm) |

We investigated how the pressure influences frictional behavior of the molecules, how the chain length influences the shear behavior, and how the shear stress (frictional force divided by contact area) is determined.

## II. Details of Model and Simulations

**A. Molecular Model.** The model used in these simulations is composed of *n*-alkanes and two solid surfaces. The molecular model of the *n*-alkanes is the same as that used by Shin and co-workers.[27] In this model, we treat $CH_3$ and $CH_2$ as pseudo-atoms. Although Shin et al. used fixed bond lengths, we used harmonic potentials, which are taken from the AMBER force field,[28] to investigate the change of the bond length under shear. The bond stretching potentials have the following form:

$$U(b) = \frac{1}{2} k_b (b - b_0)^2 \tag{1}$$

where $k_b$ is the force constant and $b_o$ is the equilibrium bond length. The bond angle stretching potentials have the following form:

$$U(\theta) = \frac{1}{2} k_\theta (\theta - \theta_0)^2 \tag{2}$$

where $k_\theta$ is the force constant and $\theta_0$ is the equilibrium bond angle.[27] The torsion potentials are assumed to have the Ryckaert−Bellmans dihedral potential forms[29] composed of four adjacent pseudoatoms and are expressed as follows:

$$U(\phi) = \sum_{i=0}^{5} C_i \cos^i(\phi) \tag{3}$$

where $\phi$ is the dihedral angle. In this form, $\phi = 0$ or $\pm(2/3)\pi$ corresponds to trans or gauche states, respectively. The intermolecular nonbonded interaction and intramolecular nonbonded interaction, when separated by more than three bonds along the same chains, are represented by the L−J form:[27]

$$U(r) = 4\epsilon\left[\left(\frac{\sigma}{r}\right)^{12} - \left(\frac{\sigma}{r}\right)^{6}\right] \tag{4}$$

where $\epsilon$ is the depth of the energy well and $\sigma$ is a core diameter. The combination rules of $\epsilon$ and $\sigma$ are $\epsilon_{ij} = \sqrt{\epsilon_i \epsilon_j}$ and $\sigma_{ij} = (1/2)(\sigma_i + \sigma_j)$, respectively. The parameters are summarized in Table 1.

We used the following model potential function for the surface that confines the liquid films to save computational time as compared with the time needed for an atomic detailed surface model. This potential surface was developed by Padilla and Toxvaerd[23] to represent the (100) face of an fcc lattice; only a brief description is given here. The potential function is built based on the mean-field solid surface potential, in which we consider 10−4 L−J form particles on a different (100) face of the fcc lattice planes.[30] In these simulations, the *z* direction is set as the film thickness direction and the *x* direction is the sliding direction. Here $f(z)$ represents the summation of the 10−4 L−J form nonbonded interactions and $g(x, y, z)$ shows periodic roughness of the atomic level in *x* and *y* directions at height *z*. The term $g(x, y, z)$ is developed based on the higher order terms of atom−wall energy functions.[27] In eq 5, *a* is a lattice parameter, $\rho_s$ is the density of the wall, $\epsilon_w$ is the depth of the energy wall, and $\sigma_w$ is a core diameter. The combination rule is $\sigma_w = (\sigma_s + \sigma_l)$, where $\sigma_s$ is the size parameter of wall atoms and $\sigma_l$ is that of the atoms composing the films. The parameters of the wall are summarized in Table 2.

**TABLE 2: Potential Function Parameters of Wall**

| parameter | value |
|---|---|
| *a* | 1.098 $\sigma_w$ |
| $\rho_s$ | $4/a^3$ |
| $\epsilon/k$ | 300 K |
| $\sigma_w$ | 0.2985 nm |
| $z_0$ | 0.752 242 274 |

**B. Details of the Simulations.** The numbers of molecules of *n*-hexane (abbreviated as C6), *n*-dodecane (C12), *n*-eicosane (C20), *n*-hexatriacontane (C36), and *n*-tetracontane (C80) were set as 205, 125, 80, 44, and 20, respectively, so that the cell height was almost the same in all systems. The cell size was 11.9025 nm$^2$. In all simulations, the initial conformations were generated between two surfaces by the method developed by Theodorou and Suter[31] to construct well-relaxed amorphous glassy polymers. We need only briefly explain this method. In each step of the conformation generation, we use the modified rotational isomeric state conditional probabilities as follows:

$$q'_{\zeta\xi;\,i} = q_{\zeta\xi;\,i} \frac{\exp\left[-\dfrac{\Delta U_{\xi;\,i}}{RT}\right]}{\displaystyle\sum_{\xi'} q_{\zeta\xi';\,i} \exp\left[-\frac{\Delta U_{\xi';\,i}}{RT}\right]} \tag{6}$$

where *i* is bond generation number, $\xi$ is rotational state of bond *i*, $q_{\zeta\xi;\,i}$ is the probability for rotational state $\xi$ of bond *i* when the previous bond state $i - 1$ is $\zeta$ and $\Delta U_{\xi;\,i}$ is the increase in long-range interaction energy (the interactions that are not considered when the probability $q_{\zeta\xi;\,i}$ is determined) in the rotational state $\xi$. Initial positions of the molecules were randomly generated. The initial densities of each liquid, C6, C12, C20, C36, and C80 were set as 0.66, 0.75, 0.85, 0.91, and 0.91 g/cm$^3$, respectively; these are measured values at room temperature and 0.1 MPa.[32]

At first the films were compressed by 100.0 MPa at 500 K for 100.0 ps and then one of the walls was moved in the *x* direction at a constant velocity of 0.1 nm/ps (100 m/s) for 400 ps under the constant pressure of 100.0 MPa at 500 K. The pressure was calculated as the component perpendicular to the moving wall of the average force between the film and the wall per unit of area. One of the walls of C12 was also moved at

$$U(x,y,z) = \frac{2\pi\rho_s\varepsilon_w}{3}\left\{\underbrace{\left(\frac{2\sigma_w^{12}}{15z^9} - \frac{\sigma_w^6}{z^3}\right)}_{f(z)} + \underbrace{10\exp\left[-21\left(\frac{z}{a} - z_0\right)\right]\left[50\cos^2\frac{\pi x}{a} + 50\cos^2\frac{\pi y}{a} + \cos^2\left(\frac{x}{a} + \frac{y}{a}\right)\right]}_{g(x,y,z)}\right\} \tag{5}$$

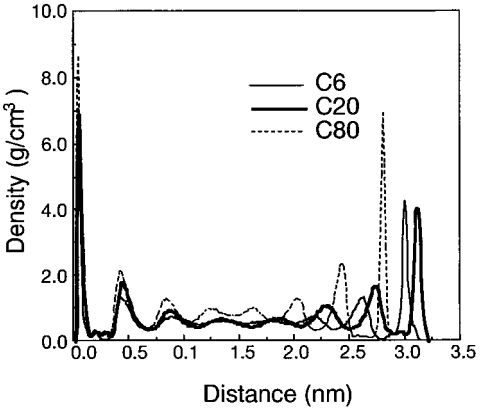


**Figure 1.** Density profiles of the films as a function of the distance from the base under 100 MPa.

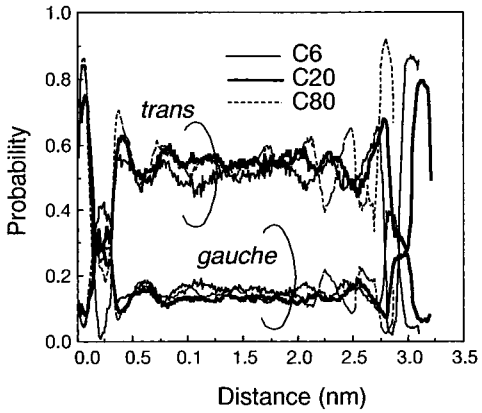


**Figure 2.** Trans and gauche probability profiles as a function of the distance from the base under 100 MPa.

different velocities, at (10, 20, 100, and 200m/s for 500ps) to get some insight into the influence of the moving wall velocity. Further, to investigate the effect of the pressure, we carried out the same simulations under a low pressure of 0.1 MPa. It took a long time to reach equilibrium under shear. Accordingly, the simulations under shear were carried out for 600−800 ps. Though the sliding speed of the SFA experiment is 6−11 orders of magnitude slower than the simulations, this sliding speed is the limit from the viewpoint of our current computational resources. Further, to use simple a *n*-alkane without solidifying, the temperature was set at 500 K.

In the simulations, the two-dimensional periodic boundary conditions were applied parallel to the film and wall surfaces. The nonbonded cutoff length was 0.9 nm. The time step was 0.5 fs, and the temperatures were controlled by Berendsen's weak coupling thermostat.[33] With this temperature control, in the sliding direction, the flow component was subtracted from the actual velocity to extract the thermal part of the velocity. The flow component was calculated as an average velocity every 3 ps as a function of the distance from the wall. The total mass of the moving wall was assumed to be 1500 (uma), and the pressure was kept constant. The initial velocities of the pseudoatoms were sampled from a Maxwell−Boltzmann distribution.

## III. Results and Discussion

**A. Shear Properties for Films at 100 MPa Pressure.** The averaged densities of each liquid C6, C12, C20, C36, and C80 at 100 MPa pressure under shear are 0.69, 0.77, 0.86, 0.90, and 0.90 g/cm$^3$, respectively. Those at 0.1 MPa pressure under shear are 0.59, 0.67, 0.74, 0.77, and 0.78 g/cm$^3$, respectively. Unfortunately, we could not find any experimental results under these conditions.

Although the calculations were carried out under high pressure and high shear rate, the bond deviations are not large compared with other simulation results.[12] In addition, no correlation appears between largeness of bond deviations and the distance from the base because of influence of the wall. From this result, we judge bond length constraint molecular dynamics to be useful even under high pressure and high shear rate. Considering that the average of the angle deviations is smaller than 0.1 rad, our use of the conventional force field in these high pressure and high shear rate simulations is acceptable.

Figure 1 represents the density profiles under the shear condition which were averaged over the last 50 ps of a 400-ps run. Hereafter, when there is no large difference between the values averaged over the last 50 ps and those averaged over the last 200 ps, we used the former. With respect to C80, the 400-ps run is supposed to be too short to reach relaxation. To confirm that there was no initial configuration dependence, we did the same simulations using two types of initial configuration. However, we found no large differences in density profiles, shear stress, and velocity profiles. Accordingly, it is reasonable to use these averaged ones. Figure 1 shows that the periodicity of the oscillations of density is ∼0.4−0.5 nm and roughly corresponds to the alkane chain width. This result indicates that the molecules tend to align in layers parallel to the surface as reported previously.[23] Each peak is sharper than usual,[23] because strong wall−fluid interaction parameters are used. The asymmetry of Figure 1 is caused by only the upper wall sliding and moving to control the pressure. Figure 1 also shows that the peaks of density profiles inside of the films are stronger when the chain length is longer. It is interesting to note that in simulations using a bead−spring model for the confined polymer, the peaks of the density profiles are weaker when the chain length is longer.[34] We think the difference is caused by the potential forms of the bond bending angles and bond torsion angles, which play an important role in determining the density profiles. Figure 2 shows averaged trans and gauche probabilities as a function of the distance from the base. The trans probability of the layers closest to the walls in each system is higher than the probabilities of inner parts of the film. This result indicates that the closest layers are closely packed to the walls. Figure 2 also shows that the trans probabilities in the layers closest to and next closest to the walls become higher with increasing chain length. This result suggests that the longer chain systems are tightly stratified.

The fact that shear stress dropped with increasing shear rate caused the experimentalists to suggest that layers were formed.[8] We calculated molecular order using the order parameter defined as the largest eigenvalue of the ordering matrix $Q$:[35]

$$Q_{\alpha\beta} = \frac{1}{2N}\sum_i (3e_{i\alpha}e_{i\beta} - \delta_{\alpha\beta}) \qquad \alpha, \beta = x, y, z \qquad (7)$$

where $e_{i\alpha}$ represents the unit vector element of the $i$th bond of the carbon and $N$ is the number of the bonds. Figure 3 shows the order parameters for C12. First and second layers represent the layers that constitute the density peaks closest to and next closest to the moving wall in Figure 1, respectively. The time steps from −100 ps to 0.0 ps are during the compressing process. As seen in Figure 3, the order parameter of the first layer does not change with time; that is, the molecules do not tend to order themselves. However, the order parameter for all molecules

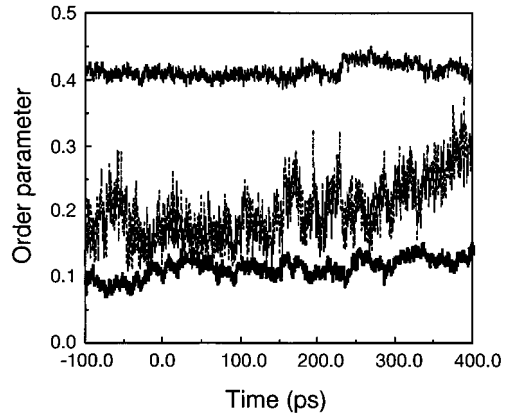


**Figure 3.** The time evolution of order parameter of C12 under 100 MPa. The thin solid line represents the order parameter of the first layer and the dashed line represents that of the second layer. The thick solid line represents the summed up result for first layer, second layer, and all other layers.

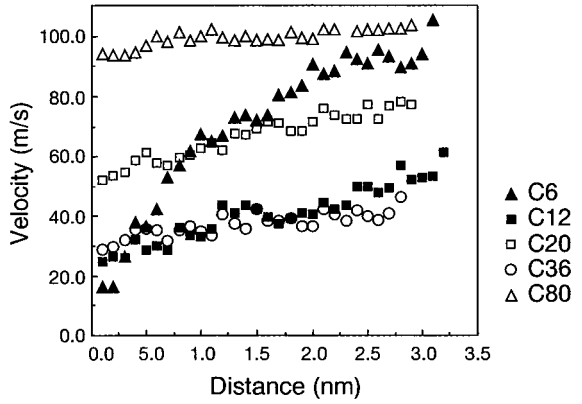


**Figure 4.** The $x$ component of the velocities ($V_x$) of each molecule as a function of the distance from the base under 100 MPa.

and for the second layer increase slightly. Further, we calculated the cosine of the $x$ axis and the eigenvector of the largest eigenvalue, which represents the direction of the molecular order, to investigate whether the molecules tend to order themselves in the sliding direction ($x$ axis). There are no increases of cos $\theta$ not only for the first layer, but also for the second layer and all of the molecules; that is, molecules do not tend to order in the sliding direction for any chain lengths. Other simulation results of the bead−spring model also find no alignment under shear.[15,18,22]

The velocities of each molecule were averaged as a function of the distance from the base and are shown in Figure 4. For all systems, except C6, the velocities of the molecules closest to the moving wall are slower than 100 m/s (= the moving wall velocity) and those closest to the base are faster than 0.0 m/s (= base velocity). That is, in all systems, except C6, the film slips past the two walls. These interfacial slips have also been observed previously in confined shear simulations of bead−spring chains[15,16,22] and hexadecane[17] and in an experiment with polydimethlsiloxane.[37] These slip conditions have been experimentally interpreted as attributable to molecules aligning in layers.[8] However, Figures 3 and 4 show molecular alignment is not always necessary for the slip conditions, which was found true in the previous simulations.[15,22] Figure 4 also shows that the shear rate is smaller when chain length is longer.

To clarify why the film slips so much at the walls, we investigated the shear stress, shear rate, and viscosity of the films. These results are summarized in Table 3. The viscosity

**TABLE 3: Shear Stress, Shear Rate, and Viscosity under 100 MPa**

| molecule | shear stress (MPa) | shear rate (1/s) | viscosity (Pa·s) |
|---|---|---|---|
| C6 | 5.50 | $2.30 \times 10^{10}$ | $2.74 \times 10^{-4}$ |
| C12 | 13.5 | $8.74 \times 10^{9}$ | $1.54 \times 10^{-3}$ |
| C20 | 13.4 | $7.78 \times 10^{9}$ | $1.72 \times 10^{-3}$ |
| C36 | 13.9 | $7.43 \times 10^{9}$ | $1.87 \times 10^{-3}$ |
| C80 | 13.9 | $2.41 \times 10^{9}$ | $5.63 \times 10^{-3}$ |

dependence on shear rate was calculated by the following equation:[38]

$$\eta = F_{xz}/\dot{\gamma} \tag{8}$$

where $F_{xz}$ is shear stress, the necessary force to move the one of the walls at a constant velocity in the sliding direction divided by the contact area and $\dot{\gamma}$ is shear rate, given by $V_x$/dz in Figure 4.

Table 3 shows that the viscosity is larger when the chain length is longer. Unfortunately, we could not find any experimental values of viscosities under these conditions. However, considering that the bulk viscosity of C12 at room temperature is 0.001 Pa·s,[9] and the bulk viscosity of C12 of the same molecular model under the same condition is 0.0015 Pa·s and that the viscosity tends to increase with longer chain lengths in Table 3, we think the results are reasonable. Table 3 also shows that the shear stress is almost the same, except for C6. If there are no slips, then $\dot{\gamma}$ equals the velocity of the moving wall divided by the film thickness, and the shear stress will be larger with higher viscosity. However, in these systems, the shear rate is slower as the chain length becomes longer and the shear stress is almost the same independent of chain length. We deduced the following from these findings. The upper limit of the shear stress is determined by the interfacial interaction energy between walls and the film. If the interaction energy between them is not large enough, the shear stress between them cannot give enough force to the film to get a uniform shear rate. Accordingly, interfacial slips between the film and the walls occur. That is, the shear stress is determined as necessary force for the film to slip past the walls. Further, these values do not depend on the chain length constituting the film, because the interfacial interactions energy is almost the same, independent of the chain length. Previous simulation results that as the wall fluid interaction is increased, the degree of interfacial slips decreases, are also explained, further supporting the present results.[17] Stevens et al.[17] explained that the interfacial slip occurs when the fluid cohesion is relatively stronger than its adhesion to the wall. Our conclusions agree with those of Stevens et al., as discussed later. The shear stress of C6 is smaller than the values for the other molecules, which is expected to be caused by the smaller interfacial interaction energy of the former and the occurrence of less interfacial slip in this case, as seen in Figure 4.

To prove the aforementioned deductions, we carried out the same simulations for C12 at different velocities. These results are summarized in Table 4 and they support the aforementioned deductions. At low velocities (10 and 20 m/s), no interfacial slip between the film and walls is seen. Moreover, the shear stress and shear rate at 10 m/s are almost half the values at 20 m/s, as expected for a Newtonian fluid with no slip. In contrast, slip is seen at 100 and 200 m/s and the shear stress is almost the same at these two velocities. The viscosities of each velocity are almost the same, shear thinning is not observed, and the film behaves like a Newtonian liquid in this slider velocity range. The results in Table 4 indicate that when the required shear

**TABLE 4: Averaged Shear Stress, Shear Rate, and Viscosity under 100 MPa for C12**

| wall velocity (m/s) | shear stress (MPa) | shear rate (1/s) | viscosity (Pa·s) |
|---|---|---|---|
| 10.0 | 4.64 | $3.60 \times 10^9$ | $1.29 \times 10^{-3}$ |
| 20.0 | 9.60 | $7.19 \times 10^9$ | $1.34 \times 10^{-3}$ |
| 100.0 | 13.5 | $8.74 \times 10^9$ | $1.54 \times 10^{-3}$ |
| 200.0 | 13.3 | $9.56 \times 10^9$ | $1.39 \times 10^{-3}$ |

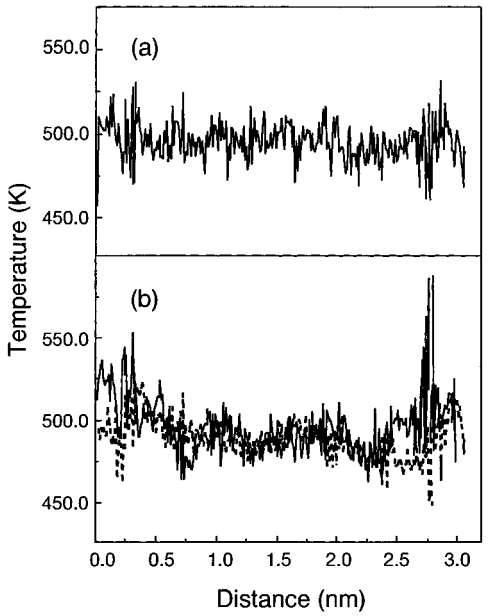


**Figure 5.** The temperature profiles of C20 at (a) 10 m/s and (b) 100 m/s (dashed line), and 200 m/s (solid line) as a function of the distance from the base after a 600-ps run.

stress for the film to consist of uniform shear rate becomes larger than the stress that the moving wall can give as frictional force per area, the film slips past the two walls and both the shear stress and shear rate are almost independent of the moving wall velocity. Thompson and Troian[36] have observed a nonlinear relationship between the amount of slip and the local shear rate around the maximum limit of the critical shear rate with the bead−spring model. The nonlinear relationship is expressed as $L_s = L_s^o\ (1 - \dot{\gamma}/\dot{\gamma}_c)^{-1/2}$, in which the film remains Newtonian.[36] The parameters $\dot{\gamma}_c$ and $L_s^o$ are limiting values, $\Delta V = L_s\dot{\gamma}$ in which $\Delta V$ is the velocity difference between the slider and the layers closest to the film. The nonlinear relationship is rewritten as $L_s = L_s^o\ (1 - F_{xz}/F_{xzc})^{-1/2}$, where $F_{xzc}$ is maximum shear stress. This equation indicates that a little increase of the shear stress is observed after interfacial slips begin to appear. To confirm that this equation is valid for simulations, the number of our simulation cases is too small. Because errors of real atom simulations are larger than those of the bead−spring model, many simulation results are necessary to confirm this equation. However, it is possible that the momentum transport limit is influenced by relative velocity of the slider to that of the layer closest to the slider because the static and dynamic interaction between slider and the film surface is probably a little different.

Figure 5 shows the temperature profiles C20 at (a) 10 m/s (solid line) and (b) 100 m/s (dashed line), 200 m/s (solid line) after a 500-ps run. The temperature profile for 10 m/s, which is the no slip condition, is almost uniform. The work of the slider is used to get uniform shear rate, and the thermal energy by friction (velocity gradient) is uniform. On the other hand, temperatures of the parts close to the walls for 100 and 200 m/s, which have interfacial slips, are higher than for inner parts of the film This tendency is noticeably stronger for 200 m/s. We used Berendsen's thermostat, so the temperature is not accurate, but the tendency is useful. These results indicate that the excess work that is not used to get a shear rate of the film by increasing slider velocity is converted into thermal energy at the interfaces.

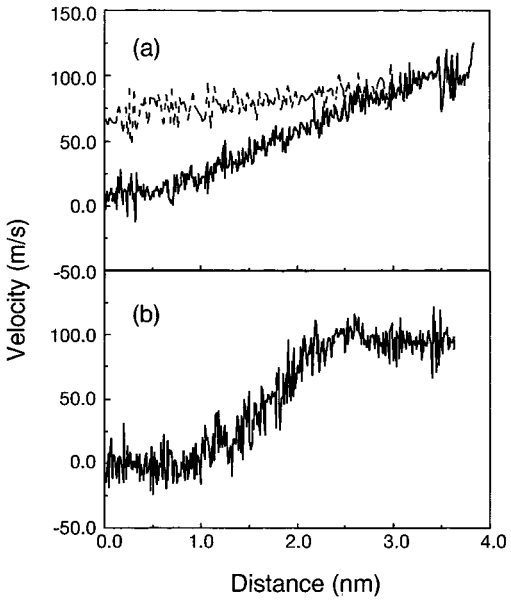


**Figure 6.** (a) The $x$ component of the velocities ($V_x$) of C12 (solid line) and C80 (dashed line) as a function of the distance from the base under 0.1 MPa. (b) The $x$ component of the velocities of C20 as a function of the distance from the base under 0.1 MPa.

Khare et al.[16] observed that the slip velocity, which is defined as the difference between the actual wall velocity and the velocity obtained by linearly extrapolating the velocity profile to the walls, monotonically increases with molecular length and reaches an approximately constant value for length longer than entanglement ($N = 50$) in the bead−spring chains. They concluded that the interfacial slips has its origins in the conductivity of molecules. Because they did not give shear stress values, we can only speculate that the change of slip velocity, that is the change of interfacial slips, is explained by changes in viscosity. The viscosities of the bead−spring chains increase motonically and interfacial slips also increase monotonically.

The following may be reasons why the film slips past the two walls. One is that the moving wall velocity is too fast, as already mentioned. The other is that the pressure is too high. Under high pressure, the energy to make a certain velocity gradient is large, because molecules become closer together and the intra- and intermolecular interaction energies become higher, so it is difficult to change the molecular packing. Because calculations at slow moving wall velocity require more calculation time to get reliable results and therefore are more expensive, it is difficult to investigate the influence of the lower shear rate. Accordingly, to postulate whether the shear stress change depends on the chain length under low pressure, we did the same simulations at 0.1 MPa.

**B. Shear Properties for Films at 0.1 MPa Pressure.** Figure 6 shows the component of the velocities for the $x$ direction of (a) C12 (solid line), C80 (dashed line), and (b) C20 systems under 0.1 MPa, which were averaged in the last 100 ps as a function of the distance from the base. The velocity profile of C6 is similar to that of C12 and that of C36 is similar

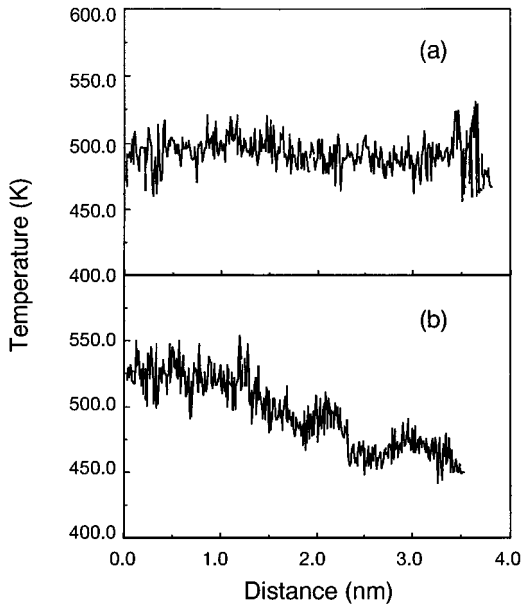


**Figure 7.** The temperature profiles of (a) C12 and (b) C20 after a 600-ps run.

to that of C20. In all of the systems except C80, the molecules closest to the moving wall have the same velocity as the moving wall (=100.0 m/s) and those closest to the base are not moving; that is, there is no interfacial slip between walls and the film, except for C80. However, the velocity gradient depends on the distance in the longer chain C20 and C36; that is, interlayer slips within the film appear. In the same simulations for C20 at a slow moving wall velocity (10m/s), there is no slip. With longer chains, the parts adsorbed on the surface are expected to be interwined and locked, thus interlayer slips within the films are likely to appear. These interlayer slips have also been observed previously in the shear simulation of bead−spring chains.[18,22] Thompson et al.[22] also observed that the interlayer slips decreased and interfacial slips increased with increasing the load. However, most of the interlayer slips of the bead−spring model occur between the first and the second peak densities in Figure 1, because the bead−spring chain does not include an attractive force in the site−site interaction and the chain length is short (molecules are usually shorter than eicosane).

Figure 7 shows temperature profiles of (a) C12 and (b) C20. C12 has a uniform profile, whereas C20 has a high temperature in the interlayer slip regions, around 1.2 and 2.1 nm. This result indicates that the local shear rate in the interlayer slip regions are a little larger than that in the middle region of the film and the thermal energy from the friction in the former is larger than that in the latter. However, this local shear rate change is unclear from the time-averaged velocity profiles in Figure 6(b). Overall, the temperature is higher closer to the base. C36 also shows the same tendency. However, in the same kind of simulation using confined perfluroether, we got the opposite tendency. This result is expected to be caused by where the strain is stored.

The shear stress, shear rate, and viscosity under 0.1 MPa are summarized in Table 5. The shear rates were calculated by excluding the steady parts that are close to the walls in C20 and C36. The results in Table 5 show that longer chains have larger shear stress. The viscosities of C20 and C36 are lower than expected based on those of C6 and C12. We do not know whether this difference is an effect of shear thinning of C20 and C36 or from another cause or error. The results in Table 5 also show that when interlayer slips occur in C20 and C36, the shear stress is smaller than the maximum values that the slider gives. Based on the previous discussion in *Section III.A*, we conclude the shear stress of C80 is the maximum interfacial shear stress. Furthermore, the shear stress of C20 at a higher speed, 150 m/s, is almost the same as that at 100 m/s. From these results we conclude that there is a shear stress limit for the interwined and locked layer to transmit the shear stress into the inner layer. When the shear stress limit of the interwined and locked layer is smaller than the shear stress limit that the slider can give, interlayer slips appear. On the other hand, when the limit shear stress of the interwined and locked layer is larger than the limit stress that the slider can give (hereafter called the maximum interfacial shear stress), interfacial slips appears. When both limit shear stresses are larger than the stress that is necessary for getting uniform shear rate, there is no slip.

**TABLE 5: Shear Stress, Shear Rate, and Viscosity under 0.1 MPa**

| molecule | shear stress (MPa) | shear rate (1/s) | viscosity (Pa·s) |
|---|---|---|---|
| C6 | 2.33 | $2.70 \times 10^{9}$ | $8.63 \times 10^{-5}$ |
| C12 | 5.38 | $3.25 \times 10^{10}$ | $1.66 \times 10^{-4}$ |
| C20 | 8.70 | $9.12 \times 10^{10}$ | $9.54 \times 10^{-5}$ |
| C36 | 11.6 | $8.16 \times 10^{10}$ | $1.42 \times 10^{-4}$ |
| C80 | 14.0 | $9.25 \times 10^{9}$ | $1.51 \times 10^{-3}$ |

We need to consider the difference in molecular behaviors between high and low pressure, because the difference in pressure causes the difference in intermolecular interaction and free volume. The maximum shear stress of interwined and locked molecules (hereafter called the maximum interlayer shear stress) is larger at high pressure than that at low pressure. The maximum interfacial shear stress is not sensitive to the pressure. Accordingly, in any system except C80, maximum interfacial shear stress is larger than that of the slider, and interfacial slips occur. For C80, even at 0.1 Mpa, the maximum interlayer shear stress is larger than maximum interfacial shear stress because of a high level of intermolecular interaction and physical connection by long chains, so interfacial slips appear. If the difference between these two maxima of the shear stress is small, both interfacial and interlayer slips appear under high shear rate, as shown previously.[22] The maximum shear stress difference of the slider is deduced from the interfacial interaction between the film and the slider or surface roughness.[36] However, the maximum of the interlayer shear stress remains elusive. Probably, not only intermolecular interaction but also physical connection have some relationships to this value, which is also probably sensitive to the molecular conformation.

To summarize, the moving wall velocity and the balance between interfacial interaction and intermolecular interaction and physical connection determines how the film behaves. These conditions (e.g., moving wall velocity, interfacial interaction, and intermolecular interaction) are expected to have a large influence on film behavior and cause characteristic behavior, such as high viscosity of the film, only when the film is thinner than ∼10 molecular diameters.

## IV. Conclusions

We have carried out molecular dynamic simulations of confined thin films composed of *n*-alkanes (chain length 6−80) under shear. The simulation results showed that their physical properties of the thin films were quite different at different pressures and different molecular lengths. At high pressure with a fast moving wall velocity, interfacial slips between the film and the walls were found in every system and the shear stress

was almost the same, independent of the chain length. The shear rate decreased and viscosity increased with longer molecular length. Thus, interfacial slips increased with longer molecular length. At low pressure, although interfacial slips were not found in any system except C80, interlayer slips within the film were found for long chains. In addition, more heat generated by friction is observed in interfacial and interlayer slip regions. From comparing the shear stress of the systems with interfacial slips, interlayer slips, and no slips, we made the following conclusions. Both interfacial shear stress, which the slider yielded, and interlayer shear stress, which interwined and locked layers yielded, had maximum values. When the maximum interfacial shear stress was larger than the maximum interlayer shear stress, interlayer slips appeared, and in the reverse, interfacial slips appeared. When the required shear stress for the film to get a uniform shear rate was smaller than these two maximum shear stresses, there was no slip. Although the maximum interfacial stress was not sensitive to the pressure, the maximum interlayer stress increased with increasing pressure. By changing the pressure, the kind of slips also changed. In this work, we only changed the pressure. However, if we changed the size of the interfacial interaction, we would get the same tendency regarding interfacial and interlayer slips.

**Acknowledgment.** We are grateful to Yutaka Ito of Hitachi Research Laboratory for helpful discussions.

## References and Notes

(1) Israelachvili, J. N.; McGuiggan, P. M.; Homola, A. M. *Science* **1988**, *240*, 190.
(2) Van Alsten, J.; Granick, S. *Phys. Rev. Lett.* **1988**, *61*, 2570.
(3) Mate, C. M.; McClelland, G. M.; Erlandsson, R.; Chiang, S. *Phy. Rev. Lett.* **1987**, *59*, 1942.
(4) Carpick, R. W.; Agrait, N.; Ogletree, D. F.; Salmeron, M. *Langmuir* **1996**, *12*, 3334.
(5) Chan, D. Y.; Horn, G. *J. Chem. Phys.* **1985**, *83*, 5311.
(6) Israelachvili, J. N. *J. Colloid Interface Sci.* **1986**, *110*, 263.
(7) Israelachvili, J. N.; Mcguiggan, P.; Gee, M.; Homola, A.; Robbins, M.; Thompson, P. *J. Phys. Condens. Matter* **1990**, *2*, SA89.
(8) Gee, M. L.; McGuiggan, P. M.; Israelachvili, J. N. *J. Chem. Phys.* **1990**, *93*, 1895.
(9) Granick, S. *Science* **1991**, *253*, 1374.
(10) Peters, G. H.; Tildesley, D. J. *Phys. Rev. E.* **1995**, *52*, 1882.
(11) Liem, S. Y.; Brown, D.; Clarke, J. H. R. *Phys. Rev. A.* **1992**, *45*, 3706.
(12) Mundy, C. J.; Siepmann, J. L.; Klein, M. L. *J. Chem. Phys.* **1995**, *103*, 10192.
(13) Lupkowski, M.; van Swol, F. *J. Chem. Phys.* **1991**, *95*, 1995.
(14) Harrison, J. A.; White, C. T.; Colton, R. J.; Brenner, D. W. *MRS Bulletin*, **1993**, May, 50.
(15) Thompson, P. A.; Grest, G. S.; Robbins, M. O. *Phys. Rev. Lett.* **1992**, *68*, 3448.
(16) Khare, R.; de Pablo, J. J.; Yethiraj, A. *Macromolecules* **1996**, *29*, 7910.
(17) Stevens, M. J.; Mondello, M.; Grest, G. S.; Cui, S. T.; Cochran, H. D.; Cummings, P. T. *J. Chem. Phys*. **1997**, *106*, 7303.
(18) Manias, E.; Hadziioannou, G.; Bitsanis, I.; ten Brinke, G. *Europhys. Lett.* **1993**, *24*, 99.
(19) Rhykerd, C. L.; Schoen, Jr. M.; Diestler, D. J.; Cushman, J. H. *Nature* **1987**, *330*, 461.
(20) Schoen, M.; Diestler, D. J.; Cushman, J. H. *J. Chem. Phys.* **1987**, *87*, 4464.
(21) Thompson, P. A.; Robbins, M. O. *Phys. Rev. A.* **1990**, *41*, 6830.
(22) Thompson, P. A.; Robbins, M. O.; Grest, G. S. *Israel J. Chem.* **1995**, *35*, 93.
(23) Padilla, P.; Toxvaerd, S. *J. Chem. Phys.* **1994**, *101*, 1490.
(24) Wang, Y.; Hill, K.; Harris, J. *J. Chem. Phys.* **1994**, *100*, 3276.
(25) Padilla, P. *J. Chem. Phys.* **1995**, *103*, 2157.
(26) Dhinojwala, A.; Cai, L.; Granick, S. *Langmuir* **1996**, *12*, 4537.
(27) Shin, S.; Collazo, N.; Rice, S. A. *J. Chem. Phys.* **1992**, *96*, 1352.
(28) Weiner, P. K.; Kollman, P. A. *J. Comput. Chem.* **1992**, *2*, 287.
(29) Ryckaert, J. P.; Bellemans, A. *J. Chem. Soc., Faraday Discuss.* **1978**, *66*, 95.
(30) Steele, A. *Surf. Sci.* **1973**, *36*, 317.
(31) Theodorou, D. N.; Suter, U. W. *Macromolecules* **1985**, *18*, 1467.
(32) *Aldrich Catalog Handbook of Fine Chemicals*; Aldrich Japan Inc., Tokyo, Japan, 1995.
(33) Berendsen, H. J. C.; Postma, J. P. M.; van Gunsteren, W. F.; DiNola, A. and Haak, J. R. *J. Chem. Phys.* **1984**, *81*, 3684.
(34) Bitsanis, I.; Hadziioannou, G. *J. Chem. Phys.* **1990**, *92*, 3827.
(35) Allen, M. P.; Tildesley, D. J. *Computer Simulation of Liquids*; Oxford University: New York, 1989.
(36) Thompson, P. A.; Troian, S. M. *Nature* **1997**, *389*, 360.
(37) Migler, K. B.; Hervet, H.; Leger, L. *Phys. Rev. Lett.* **1993**, *70*, 287.
(38) Evans, D. J.; Morriss, G. P. *Statistical Mechanics of Nonequibrium Liquids*; Academic: New York, 1990.